# COMSOL Implementation of Binder Jet Printing Densification Model in Automatic Valve System

R. Sun[1], H. Liu[1], H. H. Zhang[1, *]
[1]Polytechnic Institute, Purdue University, West Lafayette, IN, USA
[*] hhzhang@purdue.edu

## Abstract

Binder jet printing (BJP) is one of the additive manufacturing methods that are being widely implemented as an efficient alternative for casting and machining in the automotive industry. Sintering densification of the as-printed part (green part) adds uncertainty and possibly undesirable side effects to the final product. The purpose of the research is to perform theoretical analysis on densification mechanisms and provide an applicable shrinkage model in preparation for accurate additive manufacturing redesign. The paper presents a melting-solidification mathematical model and a COMSOL Multiphysics simulation of sintering densification process for binder jet printed valve body. In the COMSOL simulation, a 3D model was generated based on the valve body design. The melting-solidification mathematical model was analyzed through heat transfer and fluid flow modules to monitor the temperature increase and phase change during the sintering process. The model can be potentially implicated to help analyze the effect of sintering parameters to achieve an optimal binder jet printed product, both geometrically and metallurgically.

**Keywords:** COMSOL Multiphysics, Binder jet printing, valve-body, sintering densification

## I. Introduction

The function of the valve body in an automatic transmission is to trigger the clutch pack for the selected gearing with the channeling hydraulic fluid through the certain paths. One of the restrictions for the pipeline design is the casting process of the valve body. So far, die casting is the most common manufacturing method for valve body. To accommodate for the die design, the hydraulic pipeline must be located on the out-shape of the cast part, while the channels must be distributed on both sides of the two casting parts and then assembled together to achieve the function. High manufacturing cost and low yield limit the speed of valve body manufacturing.

In recent years, new additive manufacturing methods like selective laser melting, electron beam melting, and powder bed binder jet printing have been applied widely. While selective laser melting and electron beam melting have the limitation of inducing thermal residual stress and distortions due to large thermal gradients, binder jet printing (BJP) has been proved valid in replacing die casting for producing valve system.

Compared to conventional casting and machining manufacturing methods, BJP configures a component in a novel way: On a metal powder bed, a layer of liquid binder is selectively deposited, then cured; layer by layer, based on the CAD layered model, the configuration is 3D printed. Since the printed part is a porous structure of bonded metal powder (green body), sintering is needed to bring it to a fully dense body. Finally, heat treatment and post processing will be applied to achieve the finished product.

BJP presents an opportunity to renew the electro-hydraulic system design. Both the spool valves and internal piping designs will benefit from binder jet printing. Spool valves can be replaced by more integrated cartridge valves and assembled with solenoid or proportional switches. Throttling function can also be realized in the cartridge valves. A more integrated hydraulic channel layout is space and materials saving and can shorten the manufacturing cycles.

However, the challenge of BJP is the sintering shrinkage of the green body due to evaporation of the binder as well as partial melting and re-solidification of metal powders, leading to high level of anisotropy. Shrinkage analysis of different materials has been performed over the years. In the study conducted by Mostafaei in 2016 [1], binder jetting green parts with powder alloy 625 achieved a final density of 99.6%. However, porosity can still be observed in the microstructure, especially gathered on the grain boundary. In the study of Wheat et al. in 2018 [2], grade 1 commercially pure titanium powder was used for binder jetting printing. 85% final density were achieved while large pores were observed scattered inside the grains and in vicinity of the grain boundaries. Anton Jansson et al. [3] have proposed a method for determining the scale factor on shrinkage of steel binder jetting manufacturing in 2016. Its MATLAB coding was developed by analyzing over 100 samples generates the green parts dimension based on the expected final product dimension. So far, most BJP shrinkage analysis are performed on an empirical level focusing on metals with high thermal expansion rates such as stainless steel and Inconel alloy 625 [4]. In 2006, General Motor [5] proposed deoxidizing and coating the aluminum particles with Copper. The sintered part needs to go through further heat treatment in order to achieve the desired mechanical properties. However, little research on aluminum alloy powder BJP processes were reported. Binder jetting manufacturing of aluminum alloy powder has become more and more urgent and essential need of industry. Due to its low density, high strength, and the low thermal expansion rate [7], aluminum alloy powder attracts high interest in the automotive and aerospace industries. In consequence, an accurate modelling during the sintering stage of BJP is highly demanded in order to better monitor the final valve body geometric dimensions and tolerances and realize its complex functionalities in highly condensed space.

The research discussed thermodynamic mechanisms of melting stage and re-solidification stage of sintering. Mathematical models are proposed to explain the methodology for building the COMSOL simulation. The model is intended for predicting the heat transfer and geometric configuration of binder jet printed green part during the melting and solidification of sintering, as well as helping analyze the effect of different sintering parameters to achieve an optimal sintered binder jet

printed part metallurgically. The final goal is to simulate the A380 aluminum alloy valve body green part shrinkage of designed electrohydraulic features including multidimensional junction and channels, multidimensional bores with reservoir and ports, and cartridge valves and auxiliary plates.

## II. Methodology

### A. Melting Process Model

During the melting stage, the system is approximated as a one-dimensional heat conduction process in a semi-infinite slab. The model is based on the heat transfer problem and the geometry of figure 1 shows the molten and solid regions and the direction of furnace irradiation.

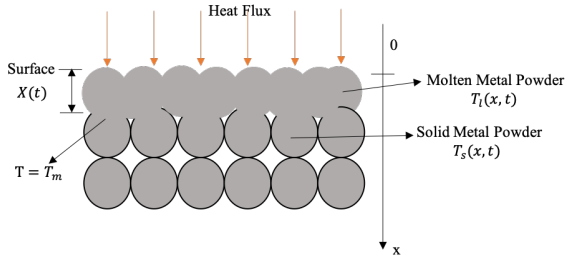


**Figure 1**. Model schematic for binder jet printed part cross section.

This study will be focused on a closed system situation, and design control laws according to the model describing this condition. Model schematic is depicted in Fig. 1, where the heat flux is parallel to X direction, while YZ plane is parallel to the metal powder layers being sintered. Metal powders will be of alloy with certain solubility and sintering parameters are within the required range. The temperature of the interface is equal to the sintering temperature. Governing Equations are as following:

$$\frac{\partial^2 T_l(x,t)}{\partial x^2} - \frac{1}{\alpha_l}\frac{\partial T_l(x,t)}{\partial t} = 0 \quad at \quad 0 \le x \le X(t) \tag{1}$$

$$\frac{\partial^2 T_s(x,t)}{\partial x^2} - \frac{1}{\alpha_s}\frac{\partial T_s(x,t)}{\partial t} = 0 \quad at \quad X(t) \le x \le \infty \tag{2}$$

$$T_l(x,t) = T_s(x,t) = T_m, \qquad x = X(t) \tag{3}$$

$$k_l\frac{\partial T_l(x,t)}{\partial x} = k_s\frac{\partial T_s(x,t)}{\partial x} - \rho L\frac{dX(t)}{dt}, \quad x = X(t) \tag{4}$$

$$-k_l\frac{\partial T_l(x,t)}{\partial x} = \eta, \; x = 0 \tag{5}$$

$$T_s(x,t) = T_0, \qquad x \to \infty \tag{6}$$

$$T_s(x,t) = T_0, \qquad t = 0 \tag{7}$$

$$X(t) = 0, \qquad t = 0 \tag{8}$$

Here $T_i$, $\alpha_i$, and $k_i$ are temperature, thermal diffusivity, and thermal conductivity of the $i$th phase, respectively, where $i = l$ and $i = s$ represent the liquid and solid phase, respectively. The term $x$ is the distance from the surface of the workpiece, $t$ is the irradiation time, $T_m$ is the melting point, $r$ is the density, $L$ is the latent heat of fusion, $T_0$ is the initial temperature, $X(t)$ is the distance from the substrate surface to the solid–liquid interface, $I$ is the heat flux power density, and $A$ is the absorptivity of materials.

Analytical solution:

$$T_l(x,t) = T_m - \frac{\eta}{k_l}[x - X(t)] + \frac{\eta}{2\alpha_l k_l\left[1 + \frac{X(t)}{\alpha_l}\frac{dX(t)}{dt}\right]} \times \frac{dX(t)}{dt}[x^2 - X^2(t)], \qquad 0 \le x \le X(t) \tag{9}$$

$$T_s(x,t) = T_m - (T_m - T_0)\left\{1 - \exp\left[-\frac{1}{\alpha_s}\frac{dX(t)}{dt}\left(x - X(t)\right)\right]\right\}, \quad X(t) \le x \le \infty \tag{10}$$

$$X(t) = \left[-\frac{b_0}{2} + \left(\frac{b_0^2}{4} + \frac{a_0^3}{27}\right)^{\frac{1}{2}}\right]^{\frac{1}{3}} + \left[-\frac{b_0}{2} - \left(\frac{b_0^2}{4} + \frac{a_0^3}{27}\right)^{\frac{1}{2}}\right]^{\frac{1}{3}} - \frac{a_l m_s}{16\eta}, \tag{11}$$

where

$$a_0 = \frac{3{a_l}^2{m_s}^2}{256\eta^2}\left(\frac{192\eta^2 t}{a_l{m_s}^2} + 31\right), \tag{11a}$$

$$b_0 = -\frac{a_l}{8\eta}\left[\frac{{a_l}^2{m_s}^3}{256\eta^2}\left(\frac{288\eta^2 t}{a_l{m_s}^2} + 47\right) + \frac{t(18\eta^2 t + 3\alpha_l{m_s}^2)}{m_s}\right] \tag{11b}$$

$$m_s = \rho[c_p(T_m - T_0) + L] \tag{11c}$$

### B. Solidification Process Model

The model consists of two parts, the first addresses the sintering time [6]. Sintering time in BJP is defined as the time heating applied to the product. The sintering time may be calculated by specifying the product thickness and solving for time.

The governing Equation of the planar front solidification of alloy is as following:

$$\frac{d\theta_s}{d\tau} = \frac{d^2\theta_s}{d\xi^2} \quad at \quad 0 \le \xi \le \xi^*(\tau) \tag{12}$$

$$\frac{d\theta_l}{d\tau} = \frac{d^2\theta_l}{d\xi^2} \quad at \quad \xi^* \le \xi \le 1 \tag{13}$$

where $\theta_s$ is the relative solidus temperature, $\theta_l$ is the relative liquidus temperature, $\tau$ is the dimensionless time, $\xi$ is the relative position, and $\xi^*$ is the relative interface position (as defined in Equations (14)-(18)).

$$\theta_s = \frac{T_s - T_0}{T_\infty - T_0} \tag{14}$$

$$\theta_l = \frac{T_l - T_0}{T_\infty - T_0} \tag{15}$$

$$\tau = \frac{\alpha t}{L^2} \tag{16}$$

$$\xi = \frac{x}{L} \tag{17}$$

$$\xi^* = \frac{x^*}{L} \tag{18}$$

The boundary conditions and initial conditions are as following:

$$\theta_s = 0 \quad at \quad \xi = 0 \tag{19}$$

$$\theta_s = \theta^* \quad at \quad \xi = \xi^*(\tau) \tag{20}$$

$$\frac{1}{Ste}\frac{d\xi^*}{d\tau} = \frac{d\theta_s}{d\xi} - \frac{d\theta_l}{d\xi} \quad at \; \xi = \xi^*(\tau) \tag{21}$$

$$\theta_l = 1 \quad at \quad \xi = 1 \tag{22}$$
$$\theta_l = 1 \quad at \quad \tau = 1 \tag{23}$$
$$\xi^* = 1 - lp \quad at \quad \tau = 0 \tag{24}$$
$$Ste = \frac{c_p(T_\infty - T_0)}{L_f} \tag{25}$$

where $Ste$ is Stefan number defined in Equation (25) and $lp$ is the relative liquid percentage.

The second part of the model calculates sintering time and creates a transient temperature profile in the metal powder layers. Binary alloy 1-D planar heat transfer model is implemented [7].

From the first part of the model, the user may specify the relative liquid percentage $lp$. The solid-liquid interface position does not therefore begin at z=0 during solidification. Governing Equations had to be modified to satisfy the initial and boundary conditions.

The analytical solution for Equation (12) and (13) with the boundary conditions (Equations (19)-(24)) is as follows:

$$\theta_s = \frac{\theta^*}{erf(\phi)} erf\left(\frac{\xi}{2\sqrt{\tau} + \frac{(1-lp)}{\phi}}\right) \tag{26}$$
$$\theta_l = 1 - \frac{1-\theta^*}{erfc(\phi)} erfc\left(\frac{\xi}{2\sqrt{\tau} + \frac{(1-lp)}{\phi}}\right) \tag{27}$$
$$\xi^* = 2\phi\sqrt{\tau} + (1-lp) \tag{28}$$
$$\theta^* = erf(\phi)\left(1 + \frac{\sqrt{\pi}}{Ste}\phi\, exp(\phi^2)\, erfc(\phi)\right) \tag{29}$$
$$t_{total} = t_{heating} + t_f \tag{30}$$

where $erfc(x) = 1 - erf(x)$ and $\phi$ can be derived from Equation (24).

$$\left\{\theta_f - erf(\phi)\left(1 + \frac{\sqrt{\pi}}{Ste}\phi\, exp(\phi^2)\, erfc(\phi)\right)\right\} \times \left\{1 - \sqrt{\pi Le}(1-k_0)\phi\, exp(\phi^2 Le)\, erfc\left(\phi\sqrt{Le}\right)\right\} = \frac{m_l C_0}{T_0 - T_\infty} \tag{31}$$

where $\theta_f$ is the dimensionless freezing point, $Le$ is Lewis number, $k_0$ is the segregation coefficient, $m_l$ is the liquidus slope, $C_0$ is the nominal composition, $T_0$ is hold temperature, and $T_\infty$ the initial temperature

With the phase transformation process thermally expressed, the mathematical model of A380 aluminum green body sintering can be derived with powder geometry, binder evaporation, and freezing zone changes, thereafter, to optimize the sintering conditions in simulation platforms.

## III. COMSOL Simulation Implementation

Using binder jet printing method, the valve body has been thoroughly redesigned. As more integrated valves have been designed to replace the spool valves and throttling function, the new hydraulic layout has been implemented and realized as a new 3D model. The model has been imported through COMSOL CAD Import Module and is shown as figure 2.

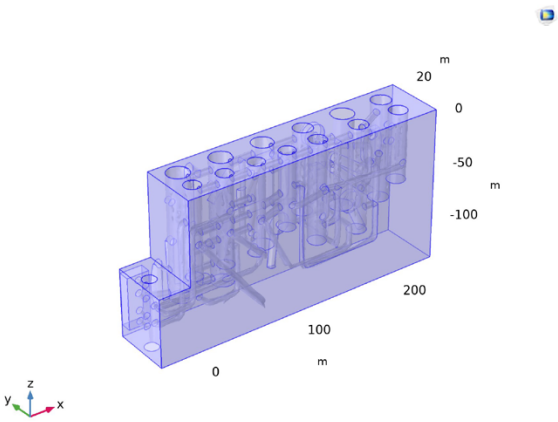


**Figure 2**. Redesigned valve body model compatible with binder jet printing manufacture process.

A380 aluminum alloy was selected as the material for the valve body 3D model. Heat capacity, thermal conductivity as well as latent heat have been defined afterwards to accommodate the numerical model. Heat Transfer and Fluid Flow modules were then utilized to simulate the sintering furnace condition based on the proposed melting and solidification mathematical models. General inward heat flux has been defined as emissivity*flux based on the grade of the sintering furnace in the research lab to replicate the actual sintering tests. Volumetric shrinkage has been simulated through deformed geometry physics. By implementing a previous solution operator, temperature solution at the previous time step was stored to determine whether volumetric shrinkage would occur.

In order to monitor the temperature and geometric evolution of each channel more closely and efficiently during the sintering process, as shown in figure 3, a simplified valve body with the same block dimensions and fewer channels has been designed to replace the full integrated model as reference. An extra fine swept mesh with triangular face meshing method was generated and a time-dependent study has been computed within a 15 min range.

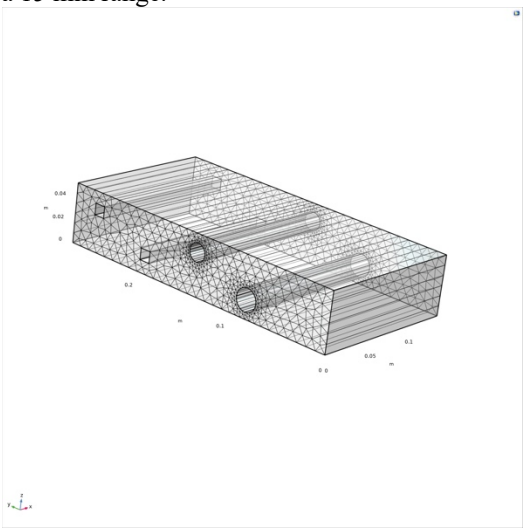

**Figure 3**. Simplified valve body model with fewer channels and extra fine swept mesh.

Temperature gradient and isothermal contour analysis were then performed as a time dependent study. In the situation where the 0.14m*0.272m*0.52m A380 aluminum block with

2 cylindrical channels and 2 rectangular channels is sintered in a 700W furnace for 0, 5, 10, 15 minutes, the simulation result is shown in figure 4 as surface temperature gradient and figure 5 as isothermal contours.

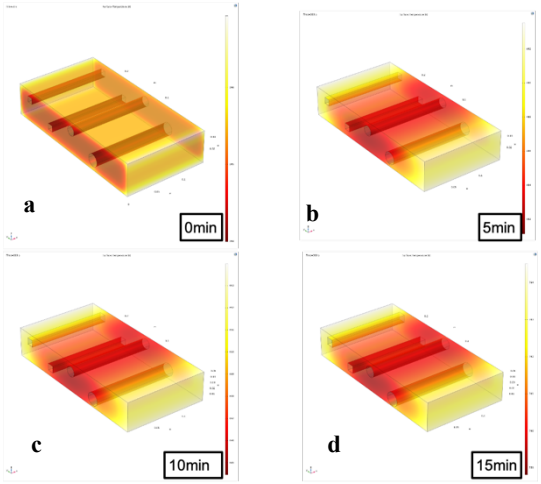


**Figure 4**. Temperature gradient of valve body after being sintered for (a) 0 min, (b) 5 min, (c) 10 min and (d) 15 min.

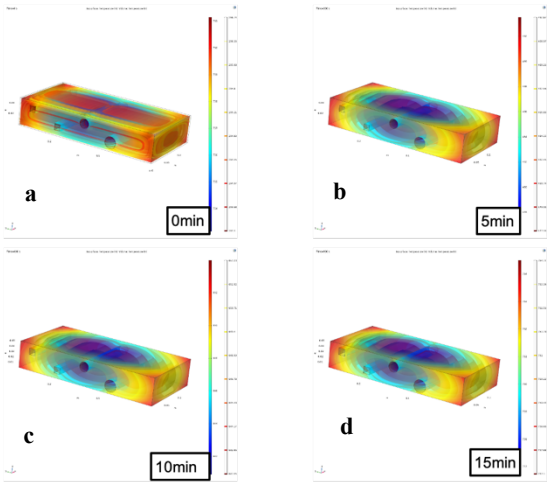


**Figure 5**. Isothermal contour of valve body after being sintered for (a) 0 min, (b) 5 min, (c) 10 min and (d) 15 min.

Shrinkage simulation of more complex features is also a necessity in order to assess the practicability of 3D printing aluminum alloy powder green part. As seen in figure 6, after 5 minutes of sintering at 800°F, compared to cylindrical channel (figure 6a), the geometric shrinkage of rectangular channel (figure 6b) is unevenly distributed mostly around the edge as well as the surface near the cavity. The inconsistent densification of rectangular cavities during melting process will highly likely lead to deformed final product. Thus, implementing cylindrical channel over rectangular channel, as well as designing more reinforcement around the cavity edges are recommended during printing stage.

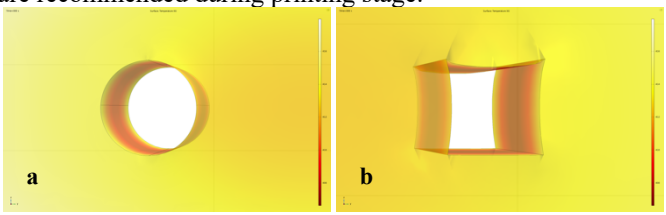


**Figure 6**. volumetric shrinkage of (a) cylindrical channel and (b) rectangular channel after being sintered for 5 min.

## IV. Results

Utilizing the point graph from 1D plot group, the temperature and the geometric evolution of a random point (figure 7) during the sintering process was analyzed as shown in figure 8 and figure 9.

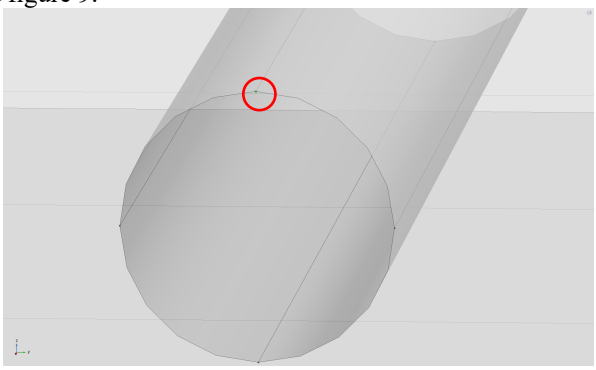

**Figure 7**. The point for analyzing the temperature and geometric evolution.

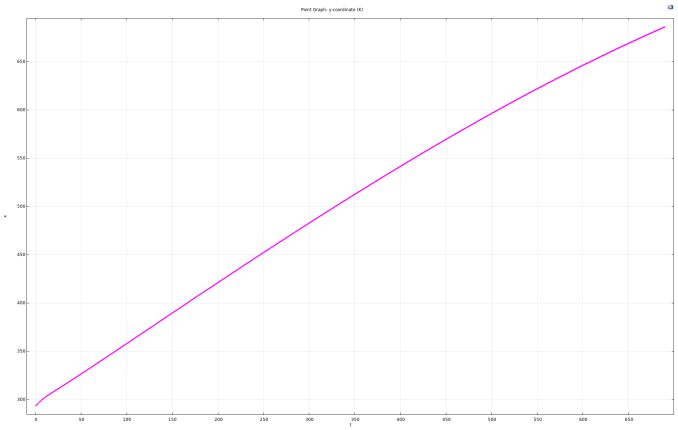

**Figure 8**. The 1D plot of temperature vs. time during sintering

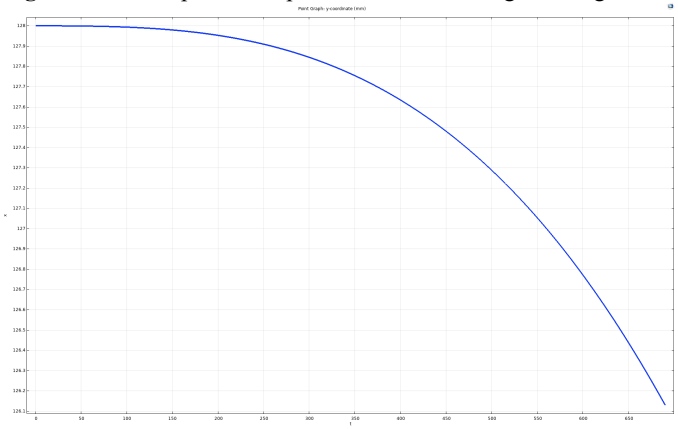

**Figure 9.** The 1D plot of y-coordinate vs. time during sintering.

In figure 8, a positive quadratic relation between temperature and time correlates with the mathematical model of melting process. The negative quadratic relation can be seen from figure 9, where the dimension of the valve body shrinks at a higher rate as time passes and temperature increases, confirming the proposed model. From this analysis, geometric evolutions of valve body channels could be back traced based on the plot data to obtain the green part volumetric design for binder jet printing.

## V. Conclusions and Discussion

The research has identified the potential of utilizing binder jet printing process as an alternative for manufacturing valve body automatic system. Mathematical models have been established to analytically express the phase transfer processes during sintering of the printed powder parts. For future analysis, sintering condition, channel design and shrinkage analysis will be vigorously tested through COMSOL Multiphysics platform before being applied to prototype production. The post sintering's metallurgical microstructures morphology, phase distribution as well as mechanical properties will also be studied.

## References


1. Mostafaei, A., Stevens, E. L., Hughes, E. T., Biery, S. D., Hilla, C., & Chmielus, M. Powder bed binder jet printed alloy 625: Densification, microstructure and mechanical properties, *Materials & Design*, **108**, 126–135 (2016)
2. Wheat, Vlasea, Hinebaugh, and Metcalfe, Sinter Structure Analysis of Titanium Structures Fabricated via Binder Jetting Additive Manufacturing, *Materials & Design*, **156**,167-183 (2018)
3. Jansson, Anton, and Oscar Edholm, Scale Factor and Shrinkage in Additive Manufacturing Using Binder Jetting, (2016)
4. Konig, Udo, Machining of Aluminum and Aluminum Alloys, *Aluminum Handbook, 1971. VEB Verlag Technik, Berlin,* 424-436 (1971)
5. "General Motors Corporation Files Patent Application for Aluminum/Magnesium 3D-Printing Rapid Prototyping." Indian Patents News [New Delhi] 2011: *Indian Patents News* (2011)
6. Sun, R., Yu, W., Zhang, H. H., Das, M., & Han, Q. Mathematical Modeling of Resistance Spot Welding. *Journal of Multidisciplinary Engineering Science and Technology, JMEST,* **6**, 2458–9403 (2019)
7. Dantzig, J. A & Rappaz, Michel, *Solidification (1st ed)*, 477-480. EPFL Press; London: Taylor & Francis [distributor], Lausanne (2009)